Internet of Things and Cloud Computing
2016; 4(5): 45-54
http://www.sciencepublishinggroup.com/j/iotcc
doi: 10.11648/j.iotcc.20160405.11
ISSN: 2376-7715 (Print); ISSN: 2376-7731 (Online)

A Sliding-Mode Control Algorithm of Self-Learning and Obstacle Avoidance for Mobile Robots

Tian Tian[1], Qiuyue Jiang[2], Zhengying Cai[1, *]

[1]College of Internet of Things Engineering, China Three Gorges University, Yichang, China

[2]College of Mechanical-Electronic Engineering, China Three Gorges University, Yichang, China

Email address:

727549631@qq.com (Tian Tian), 973787964@qq.com (Qiuyue Jiang), master_cai@163.com (Zhengying Cai)

[*]Corresponding author

To cite this article:

Tian Tian, Qiuyue Jiang, Zhengying Cai. A Sliding-Mode Control Algorithm of Self-Learning and Obstacle Avoidance for Mobile Robots. *Internet of Things and Cloud Computing.* Vol. 4, No. 5, 2016, pp. 45-54. doi: 10.11648/j.iotcc.20160405.11

Received: November 29, 2016; **Accepted**: December 13, 2016; **Published**: January 14, 2017

Abstract: It is generally very difficult to make effective obstacle avoidance for mobile robots, especially in uncertain environments. This article models the obstacle avoidance problem as a nonlinear sliding mode, using the self-learning method of non-linear system. First, a sliding mode algorithm is proposed for state dependent layers of the mobile robots, in which two kinds of boundary layers are included in, namely a sector-shaped layer and a constant layer. Second, a multi-input algorithm based on sliding-mode for self-learning of mobile robots is discussed. Some control rules are built for the self-learning and obstacle avoidance of mobile robots, and the solving steps are also presented. Last, an experiment is designed to verify the proposed model and calculate the sliding- mode control for mobile robots. Some interesting conclusions and future work are indicated at the end of the paper.

Keywords: Self-Learning, Sliding-Mode Control, Obstacle Avoidance, Mobile Robots

1. Introduction

The obstacle avoidance of mobile robots is often dynamic and uncertain, involving many nonlinear factors. Alessandro (2016) introduced dynamic stiffness model of spherical parallel robots [1]. Christopher (2016) talked about human-robot interaction in assisted personal services and factors influencing distances that humans will accept between themselves and an approaching service robot [2]. Rob (2016) indicated risk analysis for smart homes and domestic robots using robust shape and physics descriptors, and complex boosting techniques [3]. Villarreal (2016) extended off-line PID control tuning for a planar parallel robot using DE variants [4]. Rasheed (2016) described theoretical accounts to practical models with grounding phenomenon for abstract words in cognitive robots [5]. Guanglong (2016) made a model of an online method for serial robot self-calibration with CMAC and UKF [6]. Montano (2016) discussed the coordination of several robots based on temporal synchronization [7]. Yuanfan (2016) put forward a positional error similarity analysis for error compensation of industrial robots [8]. Rahmani (2016) developed a hybrid neural network fraction with integral terminal sliding mode control of an Inchworm robot manipulator [9]. Tjahjowidodo (2016) evaluated multi-source micro-friction identification for a class of cable-driven robots with passive backbone [10]. Hachmon (2016) built a non-Newtonian fluid robot [11].

Therefore, many nonlinear control methods have been applied in robot avoidance. Grubman (2016) studied partitioning de Bruijn graphs into fixed-length cycles for robot identification and tracking [12]. Duguleana (2016) illustrated neural networks based reinforcement learning for mobile robots obstacle avoidance [13]. Gundeti (2016) made a research on robot-assisted laparoscopic extravesical ureteral reimplantation and technique modifications contributing to optimized outcomes [14]. Leow (2016) extended robot-assisted versus open radical prostatectomy by a contemporary analysis of an all-payer discharge database [15]. Weichao (2016) implied two time-Scales tracking control of nonholon studied omic wheeled mobile robots [16].

The way of the robot's movement is different, and the principle is different. Tanaka (2016) gave singularity analysis of a snake robot and an articulated mobile robot with

unconstrained links [17]. Jingjing (2016) shared a control for the kinematic and dynamic models of a mobile robot [18]. Most experts supported the formation control of mobile robots. Zhe (2016) considered formation control of mobile robots using distributed controller with sampled-data and communication delays [19]. Ostafew (2016) presented robust constrained learning-based NMPC enabling reliable mobile robot path tracking [20]. Zijian (2016) offered a Force-Amplifying N-robot Transport System (Force-ANTS) for cooperative planar manipulation without communication [21].

People often applied self-learning in mobile robots to improve the performance obstacle avoidance. JianHua (2016) reviewed prospects of robot-assisted mandibular reconstruction with fibula flap, and made comparisons with a computer-assisted navigation system and freehand technique [22]. Haibo (2016) proposed a real-time, high fidelity dynamic simulation platform for hexapod robots on soft terrain [23]. Hsu (2016) indicated a particle filter design for mobile robot localization based on received signal strength indicator [24]. Mathis (2016) concerned an apex height control of a two-mass robot hopping on a rigid foundation [25].

It is generally very difficult to make effective obstacle avoidance for mobile robots, especially in uncertain environments. This article models the obstacle avoidance as a nonlinear sliding mode, using the self-learning method of non-linear system. First, a sliding mode algorithm is proposed for state dependent layers of the mobile robots, in which two kinds of boundary layers are included in, namely a sector-shaped layer and a constant layer. Second, a sliding-mode based algorithm of multi-input for self-learning of mobile robots is discussed. Some control rules are built for the self-learning and obstacle avoidance of mobile robots, and the solving steps are also presented. Last, an experiment is designed to verify the proposed model and calculate the sliding- mode control for mobile robots. Some interesting conclusions and future work are indicated at the end of the paper.

2. Self-Learning and Obstacle Avoidance for Mobile Robots

2.1. Self Learning for Mobile Robots

The term self-learning or self-teaching was used in the education without the guidance of masters, such as teachers and professors or institutions. It is general that an autodidact or an individual can choose the subject they want to study, the studying materials, studying rhythm, timetable, and so on. Similarly, the self-learning can also be used in mobile agents as robots. The mobile robot completes the autonomous movement through the cooperation of various modules. A self-learning model for mobile robots is shown in Figure 1.

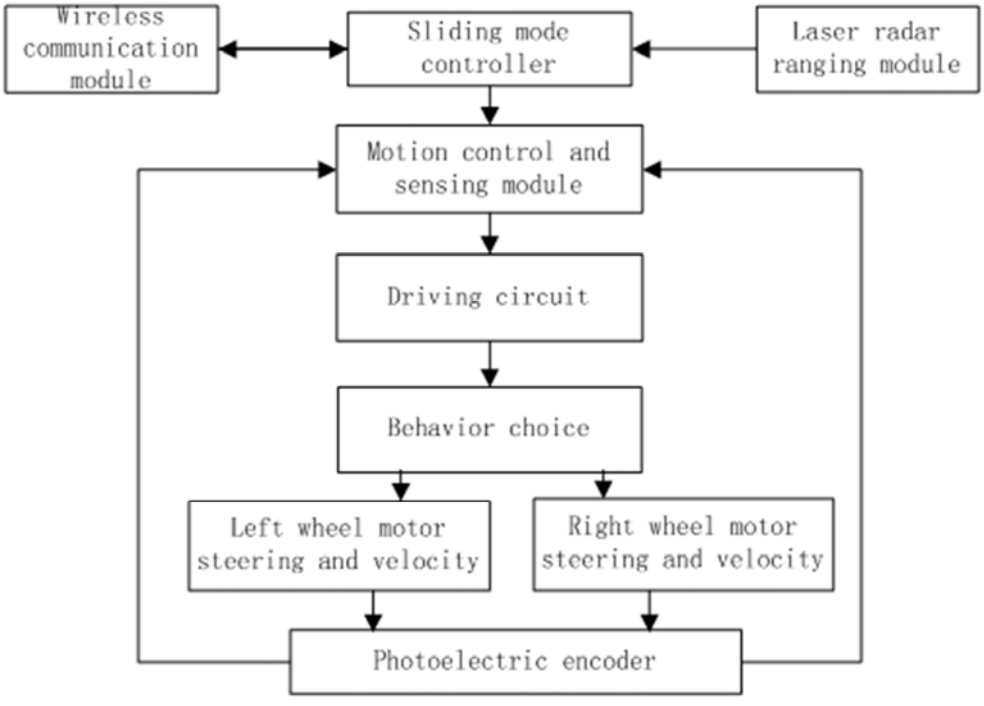

Figure 1. *A self-learning model for mobile robots.*

It indicates the control law of the ultimate bound. Yet, exponential stability of the origin is also allowed to be shown by an adjustment of the assumptions for the control and the system uncertainty. There is only parametric and uncertainty of input is supposed. Therefore, it is possible to modify the control, especially the nonlinear control model as:

Assuming u_L is the linear control element and u_{NL}^c is the nonlinear one, the coefficients $\delta_1,\ \delta_2,\ \delta_3,\ \gamma_1,\ \gamma',\ \gamma_3 \in R^+$, then the nonlinear control element is

$$u_{NL}\left(S_1(x),\varphi(x)\right)\underline{\underline{def}}\begin{Bmatrix}-\rho\left(S_1\varphi\right)B_2^{-1}H_2\,\varphi/\left[\|H_2\varphi\|+\delta_1\|S_1\|+\delta_2\|\varphi\|,\right]\left[S_1^T\varphi^T\right]^T\neq 0\\ 0, \qquad\qquad \left[S_1^T\varphi^T\right]^T=0\end{Bmatrix} \tag{1}$$

$$\gamma_1^*\underline{\underline{def}}\gamma_1^{'}+\left(\gamma_1-\gamma_1^{'}\right)\sqrt{Q_1}\Big/\left(\sqrt{Q_1}+a\sqrt{Q_2}\right),\delta_1\in R^+,\delta_2\le 0 \tag{2}$$

It is still effective for all other constraints and equations in the third and second sections. The modified control rule ω of sliding mode is worldwide Lipschitz and gradually stable.

$$\omega\underline{\underline{def}}-\omega_n/2\omega_d+\sqrt{\left(\omega_n/2\omega_d\right)^2+\delta_1\underline{\lambda}\left(H_2^{1/2}\right)/\omega_d} \tag{3}$$

$$\omega_d\underline{\underline{def}}s\,\underline{\lambda}\left(H_1^{1/2}\right)\left[\left(\underline{\lambda}\left(H_2^{1/2}\right)\right)^2\left(\gamma_1^{'}-1\right)-\delta_2\right] \tag{4}$$

$$\omega_n\underline{\underline{def}}\,\underline{\lambda}\left(H_1^{1/2}\right)\left[\left(\underline{\lambda}\left(H_2^{1/2}\right)\right)^2\left(\gamma_1^{'}-1\right)-\delta_2\right]-a\,\underline{\lambda}\left(H_2^{1/2}\right)\delta_1 \tag{5}$$

It is conditional on

$$\left[\underline{\lambda}\left(H_1^{1/2}\right)\right]^2>\delta_2\Big/\left(\gamma_1^{'}-1\right) \tag{6}$$

Specially, the state will enter the borderline layer at finite time for the positive, but the aleatoric value of the continuous control law is proposed to have two parts,

$$\mathrm{u}(\mathrm{x})=\mathrm{u}_L\left(S_1(x),\varphi(x)\right)+u_{NL}^C\left(S_1(x),\varphi(x)\right) \tag{7}$$

where u_L is the linear control element and u_{NL}^c is the nonlinear one. The nonlinear control element is

$$\mathrm{u}_{NL}^C\left(S_1,\varphi\right)\underline{\underline{def}}-\rho\left(S_1,\varphi\right)\frac{B_2^{-1}H_2\varphi}{\|H_2\varphi\|+\delta_1\|S_1\|+\delta_2\|\varphi\|+\delta_3 c} \tag{8}$$

and the coefficients $c,\delta_1,\delta_3\in R^+$, $\delta_2\ge 0$, $P_2\in R^{m\times m}$, the robustness is achieved by offsetting the coordinated uncertainties. The linear control element is

$$u_L\left(S_1(x),\varphi(x)\right)\underline{\underline{def}}-B_2^{-1}\left(\left(\Omega-\Omega^*\right)\varphi(x)+\Theta S_1(x)\right), \tag{9}$$

In a Hurwitz stable matrix and positive matrix P_2 meet the design

$$\Omega^{*T}H_2+H_2\Omega^*=-I_m. \tag{10}$$

A Lyapunov function $V_2\left(\phi(t)\right)$ for the analysis of space dynamic range (9) of a Lyapunov function $V_1\left(z_1(t)\right)$ in the zero dynamic space (10) is given through $Q1$, in which the positive definite array $P_1\in R^{(n-m)\times(n-m)}$ fulfills

$$H_1\sum+\sum^T H_1=-I_{n-m} \tag{11}$$

and an additional implicit uncertainty bound is forced which uses the largest Eigen value $\overline{\lambda}$ of a real symmetric array,

$$\overline{\lambda}\left(H_1\tilde{\sum}+\sum^T H_1\right)<0, \tag{12}$$

in order to ensure the solidity of the sliding mode (12). This occupation $\rho(z_1, \varphi)$ is defined as

$$\rho\left(z_1,\varphi\right)\underline{\underline{def}}\left[\frac{\gamma_1^*(Q_1,Q_2)}{\sigma}\right]\left[\eta_1\|H_2\varphi\|\right.$$

$$\left.+\left(\eta_2+\eta_3\right)\|z_1\|+\left(\eta_4+\eta_5\right)\right],\eta_1,,,,,\eta_5\ge 0. \tag{13}$$

A real, symmetric array is used to define the worth of the smallest Eigen value λ

$$\sigma\underline{\underline{def}}\inf_{G_1}(\underline{\lambda}(I_m+(\overline{F}_1/2)B_2^{-1}+(B_2^{-1})^T(\overline{F}_1^T/2)>0. \tag{14}$$

A scalar constant σ is as everyone knows from references, which has been told to deal with the uncertainty of input distribution matrix G_1 by wanting $\sigma > 0$ for G_1. The nonlinear controller part of multiplication $\gamma * 1 > 1$ has been formerly measured to be a constant, therefore,

$$\gamma_1^*\underline{\underline{def}}\gamma_1^{'}+\frac{(\gamma_1-\gamma_1^{'})\sqrt{Q_1}}{\left[\sqrt{Q_1}+a\sqrt{Q_2}+c\,\underline{\lambda}(Q_2^{\frac{1}{2}})/\sqrt{2}\right]},\gamma_1\ge\gamma_1^{'}>1, \tag{15}$$

In which it is positive scalar for γ. As a result, a control constant ω of the definition of the sliding layer for the state is necessary and can be defined as

$$\omega\underline{\underline{def}}-\omega_n/2\omega_d+\sqrt{(\omega_n/2\omega_d)^2+\delta_1\,\underline{\lambda}(H_2^{1/2})/\omega_d}, \tag{16}$$

where

$$\omega_d\underline{\underline{def}}2a\,\underline{\lambda}(H_1^{1/2})\left[\left(\underline{\lambda}\left(H_2^{1/2}\right)\right)^2\left(\gamma_1^{'}-1\right)-\left(\delta_2+\delta_3\right)\right],$$

$$\omega_n\underline{\underline{def}}\left(H_1^{1/2}\right)\left[\left(\underline{\lambda}\left(H_2^{1/2}\right)\right)^2(\gamma_1-1)-(\delta_2+\delta_3)\right]-2s\,\underline{\lambda}\left(H_2^{1/2}\right)\delta_1$$

From these words, the symmetric positive definite matrix

is the definition of $P_1/2$. And such that a symmetric positive definite matrix P is the definition of $P = P_1/2$. Assuming that it is always possible for the factorization, the constant ω has to be positive, which can be assured by the constraint

$$\left(\lambda\left(H_2^{1/2}\right)\right)^2 > (\delta_2 + \delta_3)/\left(\gamma_1' - 1\right). \tag{17}$$

In this case, designing small enough ω is possible. So as to, $\bar{\vartheta} > 0$,

$$0 < \bar{\vartheta} < -\lambda\left(H_1^{1/2}\sum H^{-1/2} + H_1^{-1/2}\sum{}^{T} H_1^{1/2}\right) \tag{18}$$

and a minimal value is existed

$$\xi_{\sum, \mathbf{A_{12}}}^{\mathbf{min}} = \inf_{\sum, A_{12}}(\xi) \geq 0 \tag{19}$$

meeting the array unfairness

$$M(\xi) \leq 0, \tag{20}$$

Being paid attention to, it is always feasible to find parameters with the assumption that (19) and (20) hold

$$\omega > 0,\ \bar{\vartheta} > 0, \xi_{\sum, A_{12}}^{\min} \geq 0; \tag{21}$$

2.2. Obstacle Avoidance for Mobile Robots

Normally obstacle avoidance of mobile robots is taken into account to be different from path planning because the latter is usually implemented by a reactive control law. While the obstacle avoidance involves the pre-computation of an obstacle and based on which the path controller can then direct a robot around the obstacle. It will regard linear and uncertain systems as the form

$$\dot{y} = G(x, y, u)u + F(x, y) + Ay + Bu, \tag{22}$$

In which controlled parameters are $x \in R^n, u \in R^m$, and the (A, B), which is a known matrix pair, and is assumed to be controlled by the full rank of B. Unknown functions F and G are expressed in systems with disturbances, uncertainties, and nonlinearities, in which function $G(t,x)$ can be decomposed into

$$G(x, y) = G_1(x, y) + G_2(x, y) \tag{23}$$

$G(x, y)$ represents matched actuator uncertainty: $R \times R^n \times R^m \to I(B)$, in which $I(B)$ is the range space of input array $B's$. Besides, matched and unmatched parametric uncertainty is defined by

$F_1(\cdot,\cdot)$:R×R×R $^{\mathbf{n}} \to$ R $^{\mathbf{n}\times n}$.

Although, it is a continual bounded disturbance for $F_2(.,.): R \times R_n \to R^n$.

The bounds of the uncertainty are known to K_{F1}, K_{F2}, K_G. And there are

$$\|F(x, y, u)\| < K_F, \|G_1(x, y)\| < K_{G_1}, \|G_2(x, y)\| < K_{G_2}. \tag{24}$$

Ensuring existence of solution makes the usual Caratheodory condition for

$F(t, x) + G(t, x, u)u$.

From reference 3,9 and 13, it indicates that there is always a linear transformation $\tilde{T}$ to design the sliding-mode dynamics.

$$\bar{S} = \bar{T}y = \begin{bmatrix} S_1 \\ \varphi \end{bmatrix}, \tag{25}$$

where

$$\dot{S}_1(\mathbf{x}) = \bar{G}_2 + \bar{A}_{12}\varphi(x) + \sum S_1(x),$$

$$\varphi(x) = \left(B_2 + \bar{F}_1\right)u + \bar{F}_2 + (\Omega + \Delta\Omega)\varphi(x) + (\Theta + \Delta\Theta)S_1(x),$$

$$\sum \underline{\underline{def}} \sum + \Delta\sum, \bar{A}_{12} \underline{\underline{def}} A_{12} + \Delta A_{12},$$

The sliding surface is embedded in the selected features of T and matrix, which can be arbitrarily designated. The set defines the ideal sliding mode

$$\left\{\bar{S} = \left[S_1^T \varphi^T\right]^T \in R^n : \varphi = 0\right\}. \tag{26}$$

The arrays $\Delta\Theta \in R^{m\times(n-m)}, \Delta\Omega \in R^{m\times m}, \Delta\Sigma$ and ΔA_{12} are obtained from the transformation $\tilde{T}\ F_1\ \tilde{T}\ -1$. Uncertainty of parameter matching of the system matrix A is expressed, and A_{12} is defined as the uncertainty of parameter unlatching of the system matrix. The matched uncertainty $G_1 \in R^{m\times m}$ is the uncertainty or nonlinearity in the input matrix. The input matrix follows from the transformation T_G. Matched and non-matched uncertainties of G_2 and F_2 are T_{F2}'s interference or constant constraints and the result of uncertainty.

As for a sliding mode controller which is discontinuous control, the sliding surface can be reached in a finite time. In practice, however, the discontinuous controller can lead to control signal chattering. To this end, a continuous controller is introduced to guarantee that a small state is reached in a finite time and the state depends on the boundary layer of the sliding mode.

The continual arrays A_{12}, j = 1, 2,..., k_{A12}, and i = 1, 2..., k, are the identical size with A_{12} and the scalar functions $\lambda A_{12}, j(.,.), \lambda_{\Sigma} i(.,.)$:

$R \times Rn \to R + U\{0\}$.

3. Sliding - Mode Control for Mobile Robots

3.1. The Control Rules of Sliding Mode

The selection of the controller parameters and the guidelines should follow the following formulation. By considering (4)-(7) and the control law (9) of closed loop system structure, on the condition of $\bar{\vartheta} > 0$, the choice set of controller parameter η_1....., $\eta_5 \geq 0$ is quite large, and then there is the following result:

(I) After a limited period of time, the function

$$g(Q_1, Q_2) = Q_2(\varphi(x)) - \omega^2 Q_1(S_1(x)) \tag{27}$$

will be less cost than $c_2 \bar{\lambda}$ ($P2$)/2 after a limited duration of time, will also remain less than this constant. The performance of proposed sliding mode is a state dependent sliding mode demarcation layer,

$$a_{B_x} = \left\{ \bar{S} = \left[S_1^T \varphi^T \right]^T \in R^n : Q_2(\varphi(x)) - \omega^2 Q_1(S_1(x)) \leq c^2 \bar{\lambda}(H_2)/2 \right\}, \tag{28}$$

with the final input and the time required to be limited above

$$\forall g_{Q_1,Q_2}(x_0) > c^2 \bar{\lambda}(H_2)/2:$$

$$T\left(g_{Q_1,Q_2}(x_0)\right) = \left[\bar{\lambda}(H_2)/\gamma_3 \right] \log_e \left(2 g_{Q_1,Q_2}(x_0) \Big/ \left(c^2 \bar{\lambda}/(H_2) \right) \right) \tag{29}$$

(II) This system is in a large, eventually bounded set $\tilde{\Re}(\varepsilon) > 0, \varepsilon > 0$,

$$\tilde{\Re}(\varepsilon) \underline{\underline{def}} \left\{ \bar{S} : Q_1 \leq \nu + \varepsilon, Q_2 \leq c^2 \bar{\lambda}(H_2)/2 + \omega^2 (\nu + \varepsilon) \right\}, \tag{30}$$

This is similar to the decoupling part of the matching system component which does not match the subsystem, and it is also beneficial to prove that it has an advantage that, it can be shown as the state achieving near the sliding surface. In order to achieve this goal, the function $\mathbf{g}_{\mathbf{Q_1},Q_2}$ will be of particular concern. But, in fact it will show that $\mathbf{g}_{\mathbf{Q_1},Q_2}$ has become smaller than $c_2 \bar{\lambda}$ (H_2)/2 eventually. An high limited estimation of $Q_1(S_1(x))$ will be used for decoupling and surveying of incomparable subsystem. In the case of the entire the first part, there is

$$g_{Q_1,Q_2} > c^2 \bar{\lambda}(H_2)/2 \tag{31}$$

Therefore, they confirm the robustness, compared to matching uncertainties and disturbances, in particular, now they are selected as

$$\eta_1 \underline{\underline{def}} \max \left\{ \sup_{\bar{G}_1, \Delta\Omega} \left[1/2\bar{\lambda} \left\{ H_2^{-1} \psi^T + \psi H_2^{-1} \right\} \right], 0 \right\}, \tag{32}$$

$$\eta_2 \underline{\underline{def}} \sup_{\Delta\Theta, \bar{G}_1} \left(\left\| \Delta\Theta - \bar{F}_1 B_2^{-1} \Theta \right\| \right), \tag{33}$$

$$\eta_4 \underline{\underline{def}} \sup_{\bar{G}_2} \left(\left\| \bar{F}_2 \right\| \right). \tag{34}$$

If this is the external state dependent sliding mode layer, the η_3 and η_5 of the proceeds must ensure that the Lyapunov function $V_2(\varphi(x))$ is decreasing. What a proper choice is

$$\eta_3 \underline{\underline{def}} -\omega \left[\inf_{\Delta} \sum \left(\lambda \left(\sum {}^T H_1 + H_1 \Sigma \right) \right) \Big/ 2 \right] \left\| H_1^{-1/2} \right\| \left\| H^{-1/2}/2 \right\| + \omega^2 \sup_{\Delta A_{12}} \left[\left\| H_1 \bar{A}_{12} H_2^{-1} \right\| \right], \tag{35}$$

$$\eta_5 \underline{\underline{def}} \omega \sup_{\bar{F}_2} \left[\left\| H_1^{1/2} F_2 \right\| \left\| H_2^{-1/2} \right\| \right]. \tag{36}$$

The gains η_3 and η_5 rely on ω_2 and V_1. Outside the state-dependent layer, $Q_2(x) - \omega_2 Q_1(x)$ is negative. By applying the equations (32)–(36) and (15) to inequality (31), the upper estimate of $\dot{g}_{Q_1,Q_2}$ can be derived by (31), for nearly all x,

$$\dot{g}_{Q_1,Q_2} < -(\gamma_3/2) \left\| \varphi(x) \right\|^2 - \sigma\rho\psi\left(S_1(x), \varphi(x) \right), \tag{37}$$

here (37) was followed by it, and if

$$\left\| H_2 \varphi(x) \right\| - \frac{\delta_2 + \delta_3 c/\left\| \varphi(x) \right\|}{\gamma_1^*(Q_1, Q_2) - 1} \left\| \varphi(x) \right\| \geq \frac{\delta_1 \left\| z_1(x) \right\|}{\gamma_1^*(Q_1, Q_2) - 1}, \tag{38}$$

the term ($s_1(x)$, $\varphi(x)$) from equation (37) is positive in value. From (38) and using

$$\left\| H_2^{1/2} \varphi(x) \right\| = \sqrt{2Q_2(\varphi(x))} \ldots . and \ldots . \left\| H_1^{1/2}(x) \right\| = \sqrt{Q_1(S_1(x))}, \tag{39}$$

Where

$$\|H_2\varphi\| - \frac{(\delta_2 + \delta_3 c/\|\varphi\|)}{\gamma_1^*(Q_1, Q_2) - 1} \|\varphi\| \geq \|H_2\varphi\| - \frac{\delta_2 + \delta_3}{\gamma_1^*(Q_1, Q_2) - 1} \|\varphi\| \geq \Pi,$$

$$\Pi \underline{\underline{def}} \left[\underline{\lambda} \left(H_2^{1/2} \right) - \frac{\delta_2 + \delta_3}{\underline{\lambda} \left(H_2^{1/2} \right) \left(\gamma_1^*(Q_1, Q_2) - 1 \right)} \right] \sqrt{2Q_2}$$

$$\delta_1 \left\| S_1(x) \right\| \Big/ \left[\gamma_1^* \left(Q_1(S_1(x)), Q_2(\varphi(x)) \right) - 1 \right] \leq \Pi',$$

It can be acquired by combining the right sides of (38), (39). So as to $\Pi \geq \Pi'$ Since $\gamma_1^* > \gamma'$, (38) and (39) hold, inequality (39) is true, which means that under the supposition of (26), (37), different (39) implies that ($z_1(x)$, $\varphi(x)$) is nonnegative. The constraint (39) can be substituted by a more conservative condition, which is under the supposition (39). From (39), the fact is that

$$\left\| H_1^{1/2} \varphi(x) \right\| = \sqrt{2Q_2(\varphi(x))}, \tag{40}$$

It can show that

$$c\,\underline{\lambda}\left(H_1^{1/2}\right)+\sqrt{2Q_2}\le\sqrt{2Q_1}\left(1+c/\|\varphi\|\right)\le 2\sqrt{2Q_2}. \quad (41)$$

Later,

$$\gamma^*\left(Q_1,\ Q_2\right)\ge\left(\gamma_1\text{-}\gamma_1'\right)\sqrt{Q_1}\Big/\left(\sqrt{Q_1}+s2\sqrt{Q_2}\right)+\gamma_1'. \quad (42)$$

And (42) hold assuming $Q_1 = 0$ in this case $Q_1 = 0$ is trivial, (41), (42), and $Y=\sqrt{Q_2}\big/\sqrt{Q_1}$, equation (42) can be rearranged, by using (36) and (37) to obtain

$$Y\ge-\omega_n/2\omega d+\sqrt{\delta_1\,\underline{\lambda}\left(H_2^{1/2}\right)\big/\omega_d+\left(\omega_n/2\omega d\right)^2}=\omega. \quad (43)$$

From supposition (43), it is easy to see that

$$g_{Q_1,Q_2}>c^2\bar{\lambda}\left(H_2\right)/2, \quad (44)$$

and it has inequalities.

Additionally, the coefficients can be described as $\delta_1,\ \delta_2,\ \delta_3,\ \gamma_1,\ \gamma',\ \gamma_3\in R^+$.

3.2. Solving Steps

To provide a variety of control methods of insight function, it helps the designer to select the parameters because the various control components will check the linear and stable control of U_L in this section, and $u(z_1(x),\ \varphi(x))$ in (9) to improve the accessibility of the sliding layer. The disappearance of interference or uncertainty [G= 0, F = 0 in (1)] and $\varphi(0)$ = 0, a controller $u=-B_2^{-1}\left(\Theta S_1\left(x\right)+\Omega\varphi\left(t\right)\right)$ would retain the closed-loop control system still on the sliding plane (40).

Then the additional linear term $B_2^{-1}\Omega^*\varphi\left(x\right)$ by using a stable Hurwitz matrix Ω^*, it can be ensured that $\varphi(x)$ reductions exponentially fast in the case $\varphi(0) = 0$ and $G = 0$,F = 0. To match uncertain disturbances, the nonlinear control element *null* ($s_1(x)$, $\varphi(x)$) is employed to ensure the robustness and reach the sliding demarcation layer in the limited time.

Therefore, approximating the original continuous control in the variable structure controller will use nonlinear control elements, which should be limited to prevent the control law, and has initially established a discrete judgment for the single control without stopping input.

The function $\dot{g}_{Q_1,Q_2}$ which can be confirmed easily will always become in limited time equivalent or smaller than $c2\ \bar{\lambda}$ (P2)/2. The differential inequality can be solved by integration.

$$\dot{g}_{Q_1,Q_2}<-\left(\gamma_3/\bar{\lambda}\left(H_2\right)\right)g_{Q_1,Q_2} \quad (45)$$

Henceforth, being smaller than or equivalent to $c_2\ \bar{\lambda}$ (P2)/2, the time which is required for the function $\dot{g}_{Q_1,Q_2}$ will have an upper restriction given by (40). And then the final results allow for the incomparable. The first subsystem (43) is disconnected with the fact that the Q1 is used by the Lyapunov function. The fact is

$$Q_2-\omega^2Q_1\le\left[c^2\bar{\lambda}\left(H_2\right)\right]/2. \quad (46)$$

By using (4), (30), the constant $\bar{\ }\vartheta$ from (39) indicates that for almost all x, there is

$$\dot{Q}_1=(1/2)\begin{bmatrix}H_1^{1/2}S_1\\ H_2^{1/2}\varphi/\omega\end{bmatrix}^T\quad M\left(\xi^{\min}_{\dot{\Sigma},A_{12}}\right)\begin{bmatrix}H_1^{1/2}S_1\\ H_2^{1/2}\varphi/\omega\end{bmatrix}$$

$$-\bar{\vartheta}Q_1+\xi^{\min}_{\dot{\Sigma},A_{12}}\left[Q_2\left(\varphi(x)\right)\left(1/\omega^2\right)-Q_1\left(S_1\left(x\right)\right)\right]+S_1^T\left(x\right)H_1\dot{G}_2. \quad (47)$$

Now, in terms of the matrix M in (40), the results of the S-procedure can be applied, as it is assumed that the states will eventually enter the sliding layer.

$$Q_2-\omega^2Q_1\le\left[c^2\bar{\lambda}\left(H_2\right)\right]/2, \quad (48)$$

For almost all x, there have the following

$$\dot{Q}_1\le-\bar{\vartheta}Q_1+\xi^{\min}_{\dot{\Sigma},A_{12}}c^2\bar{\lambda}\left(H_2\right)/2\omega^2+\sqrt{2}\sqrt{Q_1}\left\|H_1^{1/2}\bar{G}_2\right\| \quad (49)$$

Therefore, in the limited time, the system will finally enter the bounded set $R(\varepsilon)$.

If the polytypic sets for $\tilde{A}_{12}$ and $\tilde{\Sigma}$, the definition of a multi - type header is known. At that moment, the value of $\xi^{\min}_{\tilde{\Sigma},\ \tilde{A}_{12}}$ can be substituted

$$\max_{[i,j]\in[1.....k_\Sigma]\times[1.....k_{A_{12}}]}\left(\inf\left(\xi\right)\big|_{\dot{\Sigma}=\Sigma^i,\bar{A}_{12}=A_{12}^j}\right) \quad (50)$$

by which ξ is the maximum values of the minimal, and ξ solves the matrix inequality (50) for

$$\bar{\Sigma}=\Sigma^i=const\quad and\quad \bar{A}_{12}=A_{12}^j=const. \quad (51)$$

From observing equations (50), (51), the problem of making a decision $\xi^{\min}_{\tilde{\Sigma},\ \tilde{A}_{12}}$ can be reduced to a $K_\Sigma\times K_{A_{12}}$ inequality matrix.

Respecting the uncertainty of the parameters and some components of the uncertainty, the input distribution matrix uncertainty $\tilde{G}_1$ is also feasible that the potentially low gain and linear control term could be used to achieve partial robustness. This is a compromise between the linear and nonlinear control unit (47)–(49), which can be obtained by adjusting the parameters of γ_3, $1\ge\gamma_3>0$, in (47) and (49) respectively. And the linear control element will not be used to achieve robustness when $\gamma_3 = 1$ which is not a linear control. The gain η_1 in (49) must be large enough to match dealing with the uncertainty. Nevertheless, achieving the sliding layer phase will extend the time, the smaller γ_3, linear control to ensure more robustness and reduce the gain η_1 when choosing $\gamma_3 < 1$. Although control signal Jitter may be reduced in this way, reachability can't be shown for $\gamma_3\to 0$.

In order to overcome the discontinuity in the nonlinear control term and to reduce the nonlinear high gains, the expression $\delta_1\|\mathbf{s}_1\|+\delta_2\|\varphi\|+\delta_3 c$ has been presented to the denominator of (18) in the nonlinear control law. Therefore, around the sliding-mode plane, the value of the nonlinear control cannot change rapidly. A suitable selection of the controller parameters can also be prevented by a discrete implementation. In particular, δ_1 and δ_3 are supposed to be large enough to be chosen for quivering suppression, then this way of suppressing and quivering contrasts with the constant demarcation around the sliding mode. The smoothing component is not constant, but with reductions of $S_1(x)$ and $\varphi(x)$. In a state-dependent sliding-mode layer, this results are defined by ω in (36), the Lyapunov matrices of H_1 and H_2, and the positive scalar c from (42). The dynamic gain γ_1^* has also an effect on the size of the sliding-mode demarcation layer (42). Before the state-dependent sliding mode layer (52) is reached, the main purpose for introducing this gain is to reduce the signal peaks of high initial control. The reaching time can involve high control effort, owing to the possibly high-gain nature of the nonlinear control component. By choosing a small value for γ_1^* ($Q1$ ($S1(x)$), $Q2$ ($\varphi(x)$)) away from the sliding-mode layer, the initial peak of the control signal can be easily reduced.

$$Q_2\left(\varphi(x)\right) >> \omega^2 Q_1\left(S_1(\mathbf{x})\right). \tag{52}$$

Step by step increasing the value of γ_1^* ($Q1$ ($z_1(x)$), Q_2 ($\varphi(x)$)), the closer the situations come to the sliding plane (45) the more reaching of the sliding-mode layer can be assured for large γ_1. By means of the scalar $s > 0$ and the smaller s, the rate of increase can be selected, the higher of which will be more the rate of increase. Nonetheless, with too small a value for s, too large a choice for γ_1 combined, it may result in control signal quivering. This is certain in the case once γ_1^* is chosen too large. From (32) to (36), it is obvious that ω should be chosen as small as possible, which is to remain stable, giving a small portion of the ultimate boundedness. The quivering of the prevention should be of sufficient value to select an upper bound limit (37) for the nominal design of the sliding mode and the linear control element. Hence, the impact of the C on the ultimate bounded set size (39), provides an upper bound for the upper limit of the upper limit for the possible values for δ_1, δ_2, δ_3. Thus, the parameter values of δ_1, δ_2, δ_3, s, γ_1 and γ_1 defining ω have to be chosen carefully and the initial selection may be

$$\delta_1=\delta_2=\delta_3>0, \gamma_1=\gamma_1^{'}>1, a>0, \gamma_3=1 \tag{53}$$

It is to achieve an academically feasible and practically rational design. Also it is possible for us to modify the parameters to find a better cooperation, which is between the Jitter, the control effort, and the time to reach the sliding mode layer and achieve the control performance.

4. Experimental Analysis

4.1. Problem Description

A model of a cart pendulum system is considered here. Derived easily from (52), the linear model (53) can be employed to compute the nonlinearities together with the linear, and an explicit nonlinear model can be and the explicit model for the parameter set $M = 0.235kg$, $m = 0.134kg$, $l = 0.281m$, $g = 9.81m/s2$. Owing to the centripetal force and the term $\dot{\theta}_2$ in (52), the nonlinearities of the explicit model aren't sector bounded. Therefore, the nonlinearities can be limited in the range $|\theta| < 10$ rad/s. Furthermore, only for defined angular rod θ, the value of $\sigma > 0$ is assured to remain positive. Therefore, the value is $\sigma = 0.234$ for $|\theta| < \pi/4$ rad.

$$\Sigma=\begin{bmatrix}-0.6 & 0\\ 0 & -0.6\end{bmatrix},\quad \Omega^*=\begin{bmatrix}-3.4 & -3.4\\ 4 & -4\end{bmatrix}$$

While achieving fast reaching of the demarcation layer, Ω^* has been optimized to reduce initial controller peaks. Hence, regarded as parametric uncertainty, the nonlinear variables are limited within the constraint for $|\theta| < \pi/4$ rad system. For attention, a reduction of the value of $\delta_3 c$ would lead to quiver owing to the gain value η_4 and the effectiveness of the 5 parameters are from the Matlab/Simulink example of the constraint system. As the control rules, there is

$$(M+m)\ddot{y}+ml\left(\ddot{\theta}\cos(\theta)-\theta^2\sin(\theta)\right)=u_1+d_1$$

$$m\left(\ddot{y}\cos(\theta)+l\ddot{\theta}-g\sin(\theta)\right)=u_2+d_2$$

For continuous demarcation, the nonlinear control variable u_{NL}^c is

$$u_{NL}^c=\frac{-\gamma}{0.235}\frac{B_2^{-1}H_2\varphi^-}{\|H_2\varphi\|+\delta}\left[7.375\|H_2\varphi\|+0.601|y|+3.051|\theta|+0.139\right]$$

Paying attention, the term $0.058\|S_1\|$ from (35) is leaving out for u_{NL}^c. Because it is to control the demarcation layer of specific and the state (33), the values of $\gamma = 1.105$ and $\delta = 0.241$ are adjusted to control the sliding mode where the demarcation layer state is dependent and dynamic comparable.

The mean of the control task is to stabilize the system at [θ, x] = [0, 0]. Acting in both actuator channels, a matched disturbance is introduced, $d_1 = 0.3 \sin(2x)$, $d_2 = 0.3 \cos(\theta) \sin(2x)$.

4.2. Experimental Results

Nevertheless, when the demarcation layer and the state dependent control are to maintain control signals without quivering characteristics, the control output can be calculated (Figure 2).

From figure 2, it can display the configuration [γ, δ] = [1.329, 0.129] to produce control signal quivering, but also for the other confirmed [γ, δ] = [1.205, 0.019], also the controller

displays the initial phase Jitter in the sliding regime, as shown in Figure 2.

Without Jitter control, simulation results show that the controller keeps the system steady over a wide range of operation. While the simulation step was limited to 1/500 sec, the controller can be redesigned according to a sampling frequency of 200 Hz. By using the linear control rule for the partial nonlinear compensation, the value of γ_3 has been set to 0.1. It means the choice has been adjusted in the state-dependent demarcation layer.

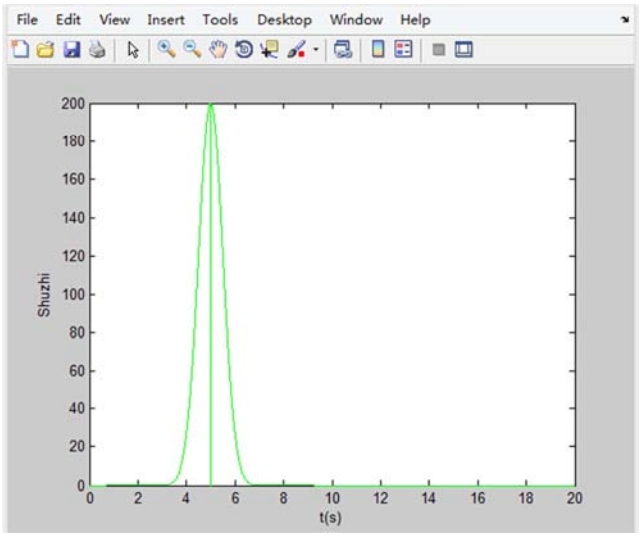

Figure 2. *Output of sliding mode control.*

As a horizontally direction, this can be interpreted as oscillating wind, so the linearized model at $[\theta, \dot{\theta}, x, \dot{x}] = [0, 0, 0, 0]$ can be given by

$$\begin{bmatrix} \dot{\theta} \\ \ddot{\theta} \\ \dot{y} \\ \ddot{y} \end{bmatrix} = \underbrace{\begin{bmatrix} 0 & 1 & 0 & 0 \\ f(N+n)/LN & 0 & 0 & 0 \\ 0 & 0 & 0 & 1 \\ -nf/N & 0 & 0 & 0 \end{bmatrix}}_{A} \begin{bmatrix} \dot{\theta} \\ \ddot{\theta} \\ \dot{y} \\ \ddot{y} \end{bmatrix} + \underbrace{\begin{bmatrix} 0 & 0 \\ -1/lN & (N+n)/nlN \\ 0 & 0 \\ 1/N & -1/N \end{bmatrix}}_{B} \begin{bmatrix} u_1 + d \\ u_2 + d \end{bmatrix}$$

The self-learning process is shown in Figure 3.

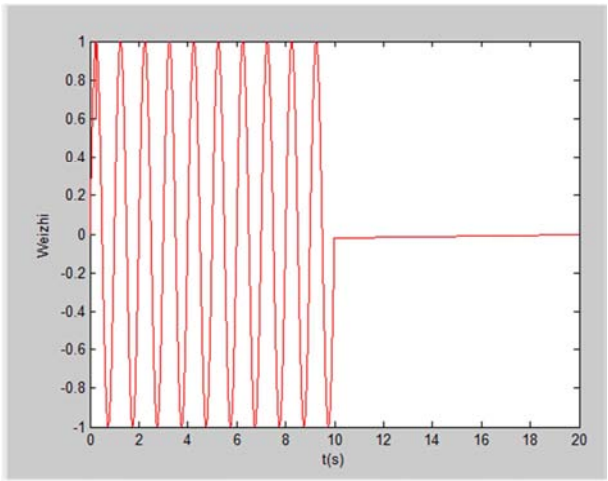

Figure 3. *The self-learning process.*

Fig. 3. shows the time response of $t(x)$, $\theta(x)$ and sliding control of inverted pendulum nonlinear function, $[\theta(0), \dot{\theta}(0), x(0), \dot{x}(0)] = [0, \pi, 0, 9]$, dual controllers with state dependent constants and demarcation layer.

Hence stable sliding-mode behavior is satisfied,

$$\rho = \left[\gamma_1^*(Q_1, Q_2)/0.\mathbf{235}\right]\left[7.375\|H_2\varphi\| + 0.601|y| + 3.051|\theta| + 0.066\|S_1\| + 0.139\right]$$

which is formed by a cart of mass M, and a light rod of length l. There is a heavy mass Mattached at the top, the end of the rod and the lever to rotate at the bottom, end fixed to the center of the cart. The cart slides in one direction, with no friction at the level of the surface. A force u_1 in the horizontal direction of movement and a torque u_2 of the cart are at the pivot of the rod, so two control signals can be availably used as actuators, respectively.

And preventing any quivering of the controller is shown in Figure 4.

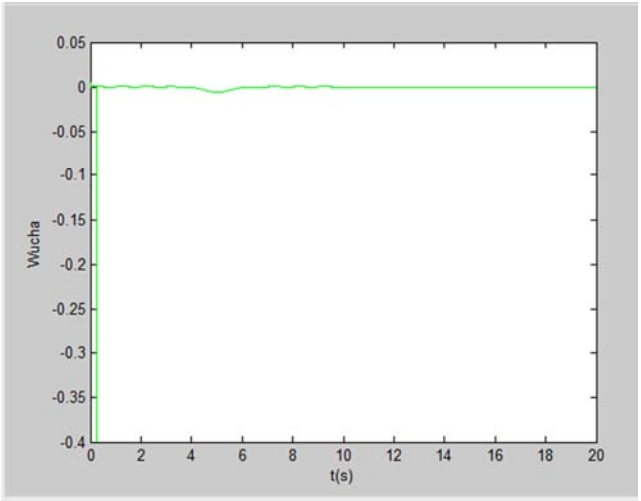

Figure 4. *Error curve.*

For the controller, sliding function with sedimentation value is close to 0, in less than 0.4 seconds (Figure 3).

From $\tilde{F}_2 = 0.105$, $\|\tilde{G}_2\| = 0.215$, $\eta_4 = 0.325$ and $\eta_5 = 0.101$. It has been employed to replace the term $\eta_2\|S_1\|$ with using $S_1^T = [t - \theta]$.

And the function

$$\sup_{\Delta\Theta F_1}\left(\left\|\left(\Delta\Theta - \bar{F}_1 B_2^{-1}\right)_{..1}\right\|\right)|x| + \sup_{\Delta\Theta F_1}\left(\left\|\left(\Delta\Theta - \bar{F}_1 B_2^{-1}\right)_{..2}\right\|\right)|\theta|$$

is to reduce the controls u_1 and u_2, and for the computation of η_1. Making the control of the sliding mode, the movement quickly reaches a mode with no shake. Sliding dynamics is especially obvious reaction to 0 (Figure 2) and the control of the state in dependent demarcation layer can cope with the matching of the interference ratio compared to the conventional nolinear control (Figure 5). Following the initial gain and the deviation, the control rule in demarcation is about 15%–31% than for the sliding-mode controller with constant demarcation.

As can be seen form the Figure 5, for the nonlinear control of inverted pendulum, time response of $t(x)$ and $\theta(x)$ in a system is based on demarcation layer in sliding mode controller using demarcation layer with dependent state and three controllers with constant.

$$\gamma_1 = 2.503, \gamma_1^{'} = 2.212, s = 60.305, \delta_1 = 0.024,$$
$$\delta_3 = 0.007, c = 1, \delta_2 = 0.$$

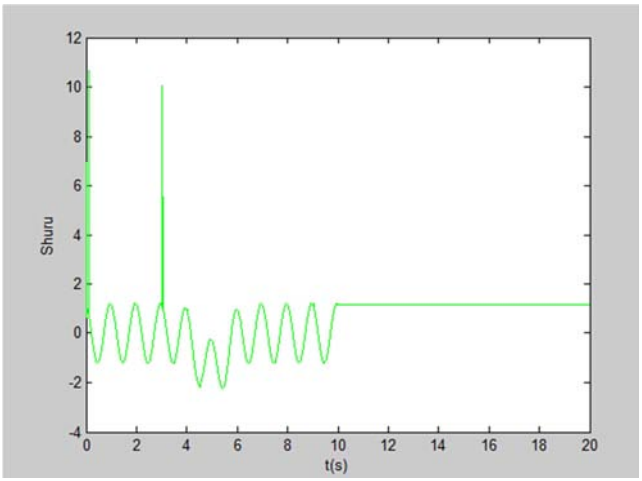

Figure 5. *Obstacle avoidance.*

For comparison, the results of reference [13] is shown in Figure 6.

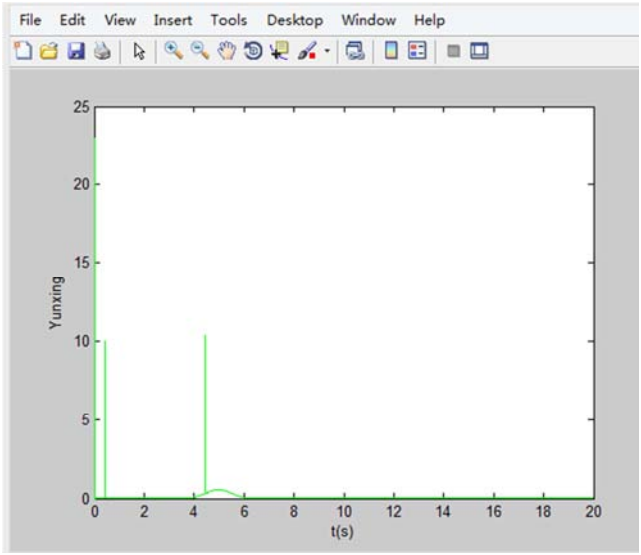

Figure 6. *Compared results in reference [13].*

As shown in Figure 6, this is a horizontal and angular position of the x and the position θ, paying attention to that the different sliding-mode control rules (16) have been tested. Specially, in order to achieve as little error as possible, the value of γ = 1.329, δ = 0.129 small value is evaluated. Therefore, the proposed sliding mode control takes advantages over the reference [13], in that the proposed model combines a constant demarcation. The greater the designer has dislodged, the more successful will the controller will be, owing to the gains η_1 and η_2.

Table 1. *Compared experiment results.*

Group	Proposed model	Reference [6]	Reference [9]	Reference [13]
Joint ($\mu mol \bullet L$)	53.05 ± 3.25	44.34 ± 2.54	45.05 ± 3.23	35.50 ± 1.28
Sliding Mode Lesion Score	20.35 ± 2.05	23.76 ± 2.78	47.05 ± 1.25	36.04 ± 3.25
Soft Lesion Score	35.04 ± 2.25	34.73 ± 3.46	64.05 ± 0.25	46.02 ± 1.27
Sliding Mode Content ($\mu mol \bullet L$)	55.05 ± 1.25	35.35 ± 5.04	45.07 ± 3.28	29.08 ± 4.25
Content ($\mu mol \bullet L$)	43.27 ± 3.27	63.05 ± 3.95	53.43 ± 2.25	47.03 ± 1.23

5. Conclusions

A sliding-mode based and state-feedback is introduced and statistically analyzed control in the paper. The unit-vector control, which is used for sliding mode control, has been changed. As a result, a state control rule of the sliding-mode is combined with both a continuous boundary layer and sector one. Bounded disturbances, bounded input uncertainty, and parametric uncertainty, have been considered as the class of uncertainty. Parametric disturbances and uncertainties are provided, and then mode rules based on sliding mode control can be effectively offset by them, and no restrictions on the boundaries of those disturbances are provided.

According to the change of the parameters of the controlled system, the self-learning control can identify, learn and adjust the control law in a timely manner, and achieve a certain performance index. The method does not need the information of the dynamic model of the controlled system, and the control gain can be adjusted according to the system performance. Moreover, the calculation is simple and the robustness is good. In this paper, the parameters of the dynamic model are estimated by the self-learning logic, which makes the control system has strong adaptability.

In future work, the bounds for input-uncertainty and unmatched parametric uncertainty, which are controlled by the proposed dynamics, should be further studied and compared. The example here is simplified to verify the sliding pattern system and will be implemented in more complex environments to demonstrate the emergence of a discrete new MIMO control scheme. In addition, the controller with state boundary layer will also be further researched to withdraw better interference suppression characteristic than a traditional controller.

Acknowledgements

This research was supported by the National Natural Science Foundation of China (No. 71471102), and Science and Technology Research Program, Hubei Provincial Department of Education in China (Grant No. D20101203).

References

[1] Cammarata, Alessandro; Calio, Ivo; D'Urso, Domenico; Dynamic stiffness model of spherical parallel robots. Journal of Sound and Vibrtion, Vol. 384, 2016, pp. 312-324.

[2] Brandl, Christopher; Mertens, Alexander; Schlick, Christopher M. Human-robot interaction in assisted personal services: factors influencing distances that humans will accept between themselves and an approaching service robot. Human Factors and Ergonomics in Manufacturing & Service Industries, Vol.26, No. 6, 2016, pp. 713-727.

[3] Dupre, Rob; Argyriou, Vasileios; Tzimiropoulos, Georgios; Risk analysis for smart homes and domestic robots using robust shape and physics descriptors, and complex boosting techniques, Information Sciences, Vol.372, 2016, pp. 359-379.

[4] Villarreal-Cervantes, Miguel G.; Alvarez-Gallegos, Jaime, Off-line PID control tuning for a planar parallel robot using,DE variants, Expert Systems with Applications, Vol. 64, 2016, pp. 444-454.

[5] Rasheed, Nadia; Amin, Shamsudin H. M.; Sultana, U.; Theoretical accounts to practical models: grounding phenomenon for abstract words in cognitive robots. Cognitive Systems Research, Vol. 40, 2016, pp. 86-98.

[6] Du, Guanglong; Shao, Hengkang; Chen, Yanjiao. An online method for serial robot self-calibration with CMAC and UKF. Robotics and Computer-integrated Manufacturing, Vol. 42, pp. 39-48, DEC 2016.

[7] Montano, Andres; Suarez, Raul. Coordination of several robots based on temporal synchronization. Robotics and Computer-integrated Manufacturing, Vol. 42, 2016, pp. 73-85.

[8] Zeng, Yuanfan; Tian, Wei; Liao, Wenhe. Positional error similarity analysis for error compensation of industrial robots, Robotics and Computer-Integrated Manufacturing, Vol. 42, 2016, pp. 113-120.

[9] Rahmani, Mehran; Ghanbari, Ahmad; Ettefagh, Mir Mohammad. Hybrid neural network fraction integral terminal sliding mode control of an inchworm robot manipulator. Mechanical Systems and Signal Processing, Vol. 80, 2016, pp. 117-136.

[10] Tjahjowidodo, Tegoeh; Zhu, Ke; Dailey, Wayne; Multi-source micro-friction identification for a class of cable-driven robots with passive backbone. Mechanical Systems and Signal Processing, Vol. 80, 2016, pp. 152-165.

[11] Hachmon, Guy; Mamet, Noam; Sasson, Sapir. A non-newtonian fluid robot. Artificial Life, Vol. 22, No. 1, 2016, pp. 1-22.

[12] Grubman, Tony; Sekercioglu, Y. Ahmet; Wood, David R. Partitioning de Bruijn graphs into fixed-length cycles for robot identification and tracking. Discrete Applied Mathematics, Vol. 213, 2016, pp. 101-113.

[13] Duguleana, Mihai; Mogan, Gheorghe. Neural networks based reinforcement learning for mobile robots obstacle avoidance. Expert Systems with Applications, Vol. 62, 2016, pp. 104-115.

[14] Gundeti, Mohan S.; Boysen, William R.;Shah, Anup. Robot-assisted laparoscopic extravesical ureteral reimplantation: technique modifications contribute to optimized outcomes. European Urology Vol. 70, No. 5, 2016, pp. 818-823.

[15] Leow, Jeffrey J.; Chang, Steven L.;Meyer, Christian P. Robot-assisted versus open radical prostatectomy: a contemporary analysis of an all-payer discharge database. European Urology, Vol. 70, No. 5, 2016, pp. 837-845.

[16] Sun, Weichao; Tang, Songyuan; Gao, Huijun. Two time-scale tracking control of nonholonomic wheeled mobile robots. IEEE Transactions on Control Systems Technology, Vol. 24, No. 6, 2016, pp. 2059-2069.

[17] Tanaka, Motoyasu; Tanaka, Kazuo. Singularity analysis of a snake robot and an articulated mobile robot with unconstrained links. IEEE Transactions on Control Systems Technology, Vol. 24, No. 6, 2016, pp. 2070-2081.

[18] Jiang, Jingjing; Di Franco, Pierluigi; Astolfi Alessandro. Shared control for the kinematic and dynamic models of a mobile robot. IEEE Transactions on Control Systems Technology, Vol. 24, No. 6, 2016, pp. 2112-2124.

[19] Liu, Zhe; Chen, Weidong; Lu, Junguo. Formation control of mobile robots using distributed controller with sampled-data and communication delays. IEEE Transactions on Control Systems Technology, Vol. 24, No. 6, 2016, pp. 2125-2132.

[20] Ostafew, Chris J.; Schoellig, Angela P.; Barfoot, Timothy D. Robust constrained learning-based NMPC enabling reliable mobile robot path tracking. International JournalL of Robotics Research, Vol. 35, No. 13, 2016, pp. 1547-1563.

[21] Wang, Zijian; Schwager, Mac. Force-amplifying n-robot transport system (force-ants) for cooperative planar manipulation without communication. International Journal of Robotics Research, Vol. 35, No. 13, 2016, pp. 1564-1586.

[22] Zhu, Jian-Hua; Deng, Jiang; Liu, Xiao-Jing. Prospects of robot-assisted mandibular reconstruction with fibula flap: comparison with a computer-assisted navigation system and freehand technique. Journal of Reconstructive Microsurgery, Vol. 32, No. 9, 2016, pp. 661-669.

[23] Gao, Haibo; Jin, Ma; Ding, Liang; A real-time, high fidelity dynamic simulation platform for hexapod robots on soft terrain. Simulation Modelling Practice and Theory, Vol. 68, pp. 125-145, NOV 2016.

[24] Hsu, Cheng-Chung; Yeh, Syh-Shiuh; Hsu, Pau-Lo. Particle filter design for mobile robot localization based on received signal strength indicator. Transactions of The Institute of Measurement AND Control, Vol. 38, No. 11, 2016, pp. 1311-1319.

[25] Mathis, Frank B.; Mukherjee, Ranjan. Apex height control of a two-mass robot hopping on a rigid foundation. Mechanism and Machine Theory, Vol. 105, 2016, pp. 44-57.